
Pyramid Convolutional RNN for MRI Reconstruction

Puyang Wang^{*†}

Department of Electrical and Computer Engineering
Johns Hopkins University
Baltimore, MD 21218
pwang47@jhu.edu

Eric Z. Chen[†]

United Imaging Intelligence
Cambridge, MA 02140
zhang.chen@united-imaging.com

Terrence Chen

United Imaging Intelligence
Cambridge, MA 02140
terrence.chen@united-imaging.com

Vishal M. Patel

Department of Electrical and Computer Engineering
Johns Hopkins University
Baltimore, MD 21218
vpatel136@jhu.edu

Shanhui Sun

United Imaging Intelligence
Cambridge, MA 02140
shanhui.sun@united-imaging.com

Abstract

Fast and accurate MRI image reconstruction from undersampled data is critically important in clinical practice. Compressed sensing based methods are widely used in image reconstruction but the speed is slow due to the iterative algorithms. Deep learning based methods have shown promising advances in recent years. However, recovering the fine details from highly undersampled data is still challenging. In this paper, we introduce a novel deep learning-based method, Pyramid Convolutional RNN (PC-RNN), to reconstruct the image from multiple scales. We evaluated our model on the fastMRI dataset and the results show that the proposed model achieves significant improvements than other methods and can recover more fine details.

1 Introduction

Magnetic Resonance Imaging (MRI) as a non-invasive approach has many advantages over other imaging techniques, such as no radiation and good soft-tissue contrast [Edmund and Nyholm, 2017, Weekes et al., 1985]. However, due to the physic limitations of MRI, the data acquisition is inherently slow, which causes patient discomfort, increases costs, and hinders MRI in many other clinical applications [Lecchi et al., 2008]. One common approach to accelerate MRI data acquisition is to take fewer measurements, generating an undersampled k-space. Recovering the image from the heavily undersampled k-space data is challenging and has been an active research field.

Compressed sensing (CS) has been accepted for MR image reconstruction in current clinical practice. In order to reconstruct the image from incoherently undersampled data, CS requires the data to be

^{*} This work was carried out during the internship of the author at United Imaging Intelligence, Cambridge, MA.

[†] These authors contributed equally.

sparse either in the original pixel domain or in a transformed domain [Candès et al., 2006]. Since very few MRI image modalities are intrinsically sparse in the pixel domain, thus identifying the optimal sparse transform is often the key ingredient in CS based methods. Those sparse transformations are often manually designed, such as total variation (TV) and wavelet transform [Ma et al., 2008, Ye, 2019]. The MRI construction with the sparse constraint can be considered as an L1 optimization problem and non-linear optimization algorithms are used to solve for the solution [Lustig et al., 2007, Fessler, 2019]. However, those optimization algorithms are usually iterative by nature and take a relatively long computation time, which hinders or even prohibits MRI in certain clinical applications. In addition, CS based methods generally include some hyper-parameters that control the degree of the smoothness due to the sparse constraint and improper values of those hyper-parameters usually result in over-smoothed images or artifacts. Therefore, it takes great efforts to manually tune those hyper-parameters in real practice for CS based methods. Due to the computational complexity as well as the tendency to introduce compression artifacts or over-smoothing, CS based approaches have taken some time to gain acceptance in the clinic and the acceleration factor has limited to around four or even less.

To avoid above drawbacks of CS, deep learning based methods have been proposed for MRI reconstruction in recent years [Selvikvåg Lundervold and Lundervold, 2018]. As a data-driven approach, deep learning can directly learn the optimal sparse transformation from the data. Additionally, it only takes one forward pass for the network to reconstruct the image in inference time and therefore is intrinsically faster than CS. However, it is a great challenge for current deep learning methods to recover the high frequency signals (i.e., fine details) from undersampled data, especially with a high acceleration rate. Nevertheless, the details in the reconstructed image are crucial for clinical diagnosis.

This motivates us to propose a pyramid convolutional RNN (PC-RNN) for MRI reconstruction, which extracts multi-scale features. Our method can recover fine details while preserving data consistency.

2 Method

Mathematically, the data acquisition process of MRI can be formulated as follows:

$$y = Ax + \epsilon, \quad (1)$$

where $x \in \mathbb{C}^M$ is the image we want to reconstruct, $y \in \mathbb{C}^N$ is the observed k-space, and ϵ is the noise. Both x and y are data from one coil and represented in vector form. A is the forward operator and often includes the multiplication of the Fourier transform matrix F , the binary undersampling matrix D and coil sensitivity matrix S . In our work, we don't use coil sensitivity maps and ignore S in the following paper. The goal of MRI image reconstruction is to estimate image x from observed k-space y . This can be preliminarily solved as an optimization problem:

$$\operatorname{argmin}_x \frac{1}{2} \|y - Ax\|_2^2, \quad (2)$$

where $\|y - Ax\|_2^2$ is often called data fidelity term.

MRI reconstruction can be considered as an inverse problems, in which the forward model is well-defined but the inverse process is ill-posed due to the information loss in the forward process as $N < M$. Therefore, solutions from direct optimization of Eqn 2 are unstable. A regularization term can be added to the objective function:

$$\operatorname{argmin}_x \frac{1}{2} \|y - Ax\|_2^2 + \lambda R(x), \quad (3)$$

where $R(x)$ is the regularization term and λ is the weight. In CS, $R(x)$ takes the form of $\|\Psi x\|_1$, where Ψ is the transformation matrix. This L1 term forces x to be sparse in the transformed domain. In deep learning, this regularization function $R(x)$ can be learned from data.

Many optimization algorithms can be used to minimize the objective function in Eqn. 3 such as gradient decent, proximal gradient descent and primal-dual optimization algorithms. As long as $R(x)$

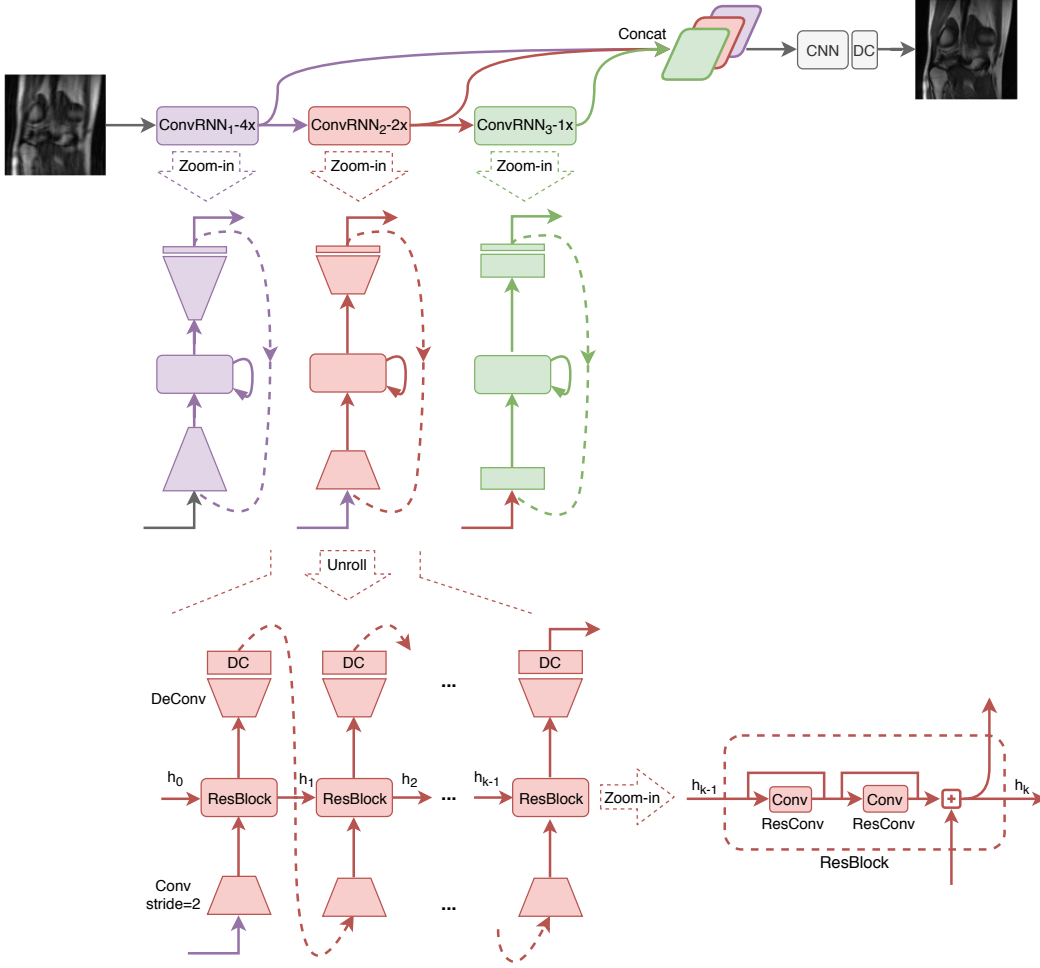


Figure 1: Proposed Pyramid Convolutional RNN (PC-RNN).

is differential, we can solve Eqn. 3 using gradient decent in an iterative fashion. For each iteration,

$$\hat{x}^{(k+1)} = \hat{x}^{(k)} + \alpha[A^T(y - A\hat{x}^{(k)}) + \nabla R(\hat{x}^{(k)})], \quad k = 0, 1, \dots, K \quad (4)$$

where k is the index for iteration and α is the learning rate.

The above iterative optimization process can be modeled by a Convolutional Recurrent Neural Network (ConvRNN) model [Qin et al., 2018] as

$$\hat{x} = \text{ConvRNN}(\tilde{x}, y, D, \theta), \quad (5)$$

where \tilde{x} is the input image (e.x., undersampled image), y is the undersampled k-space, D is the sampling mask, and θ are the parameters of the ConvRNN model. In ConvRNN, all matrix multiplications in the RNN model are replaced with convolution operations for images [Keren and Schuller, 2016, Shi et al., 2015].

2.1 Pyramid Convolutional RNN

Here, to improve the recovery of fine details, we propose to reconstruct the image at multiple scales. Consider the image x as the combination of images x_i in different scales.

$$x = f(x_1, x_2, \dots, x_s), \quad (6)$$

where x_s indicates image x at scale s and f is a function to integrate images from different scales. Then we can reconstruct each x_s as:

$$\hat{x}_s = g_s(\tilde{x}_s), \quad (7)$$

where \tilde{x}_s is the image with artefacts and g_s is the function for reconstruction. Each g_s is specialized in modeling the signal at a certain scale, especially the high frequency signals.

Based on Eqn.5,6 and 7, we propose a novel network Pyramid Convolutional RNN (PC-RNN) as shown in Figure 1. It features three specially designed ConvRNN modules to model data in different scales (ConvRNN₁-4x, ConvRNN₂-2x and ConvRNN₃-1x in the upper panel of Figure 1). Each ConvRNN module consists of an encoder g^{enc} , an decoder g^{dec} , a basic RNN cell (ResBlock) g^{res} including two residual convolutions (ResConv), and a data consistency (DC) layer, as shown in the middle panel of Figure 1. The input images are zero-filled undersampled complex images $F^{-1}D^T y$ with real and imaginary values as two channels. The output of $(k + 1)^{th}$ iteration of ConvRNN _{i} can be derived as follows:

$$x_i^{(k+1)} = DC(g_i(x_i^{(k)}, h_i^{(k)}, y, D, \theta_i)) \quad (8)$$

$$= F^{-1}[Dy + (1 - D)Fg_i^{dec}(g_i^{res}(h_i^{(k)}) + g_i^{enc}(x_i^{(k)}))], \quad (9)$$

where $h_i^{(k)} = g_i^{res}(h_i^{(k-1)}) + g_i^{enc}(x_i^{(k-1)})$ is the hidden state from previous iteration and $h_i^{(0)} = 0$. The final output after K iteration of all three ConvRNN are derived recursively:

$$x_1 = \text{ConvRNN}_1(x_0, y, D, \theta_1) \quad (10)$$

$$x_2 = \text{ConvRNN}_2(x_1, y, D, \theta_2) \quad (11)$$

$$x_3 = \text{ConvRNN}_3(x_2, y, D, \theta_3), \quad (12)$$

where $x_0 = F^{-1}D^T y$ is the zero-filled undersampled image and θ are parameters of the networks. To ensure each ConvRNN can extract features at different scales (downsampling the feature map size by 4x, 2x, 1x) and reconstruct the image accordingly, we varies the contracting and expanding factors (strides) of encoders and decoders. We use two (de-)convolution layers with stride=2 in the encoder and decoder of first ConvRNN to perform the coarse reconstruction and one or none (de-)convolution layers for second and last ConvRNN to fill in fine details. See Table S1 for details of the network architecture. Specifically, Conv(2,3,1) denotes a convolutional layer with stride of 2, kernel size of 3×3 , and zero padding size of 1, while DeConv(2,4,1) denotes a de-convolutional (transposed convolutional) layer with stride of 2, kernel size of 4×4 , and zero padding size of 1. Each (de-)convolutional layer (except the last one) is followed by a ReLU layer.

Finally, we applied a CNN module to combine the three reconstructed images x_1, x_2, x_3 and derived the final reconstruction \hat{x} :

$$\hat{x} = DC(\text{CNN}(x_1, x_2, x_3)). \quad (13)$$

Note that, for multi-coil task, we used a stack of undersampled images of all coils as the input and the network outputs the reconstructions of all coils. The final reconstruction is obtained by combining all coils using the root sum squared (RSS) method,

$$\hat{x}_{\text{rss}} = \sqrt{\sum_{c=1}^{n_c} |\hat{x}_c|^2}, \quad (14)$$

where n_c is the number of coils.

2.2 Training and evaluation

We used the knee MRI data from fastMRI competition [Zbontar et al., 2018], which includes two tasks, single-coil and multi-coil. Both single-coil and multi-coil data include 973 volumes (34,742 slices) as the training dataset and 199 volumes (7,135) as the validation dataset. The fully sampled kspace data are provided in both datasets but Emulated Single-Coil (ESC) data is used as the ground truth in single-coil task and Root-Sum-of-Squares (RSS) reconstruction is used as the ground truth in multi-coil task. Only subsampled data (i.e., no fully sampled data) are provided in the test dataset. The results of the test dataset can be evaluated on the fastMRI website.

We used the Normalised Mean Square Error (NMSE) loss and the Structural Similarity Index (SSIM) loss as our training loss. The total loss functions are derived as follows:

Table 1: Evaluation results of CS, UNet and PC-RNN on fastMRI validation data

Task	Method	PSNR		SSIM	
		4X	8X	4X	8X
Single-coil	CS	29.5	27.0	0.570	0.484
Single-coil	U-Net	31.9	29.9	0.723	0.654
Single-coil	PC-RNN	32.8	31.3	0.743	0.682
Multi-coil	CS	30.1	28.2	0.632	0.595
Multi-coil	U-Net	33.7	33.7	0.894	0.852
Multi-coil	PC-RNN	39.0	36.5	0.914	0.884

Table 2: Evaluation results of PC-RNN on fastMRI test data

Task	PSNR		SSIM	
	4X	8X	4X	8X
Single-coil	34.0	30.9	0.776	0.677
Multi-coil	39.9	36.8	0.928	0.887

$$\mathcal{L}_{NMSE}(\hat{x}, x) = \frac{\|\hat{x} - x\|_2^2}{\|v\|_2^2} \quad (15)$$

$$\mathcal{L}_{SSIM}(\hat{x}, x) = \frac{(2\mu_{\hat{x}}\mu_x + c_1)(2\sigma_{\hat{x}x} + c_2)}{(\mu_{\hat{x}}^2 + \mu_x^2 + c_1)(\sigma_{\hat{x}}^2 + \sigma_x^2 + c_2)} \quad (16)$$

$$\mathcal{L}(\hat{x}, x) = \mathcal{L}_{NMSE} + \beta\mathcal{L}_{SSIM}, \quad (17)$$

where $\|v\|_2^2$ represents squared Euclidean norm of the volume v that x belongs to, and $c_1 = (k_1L)^2$, $c_2 = (k_2L)^2$ in SSIM. In this paper, we choose a window size of 7×7 , we set $k_1 = 0.01$, $k_2 = 0.03$, and define L as the maximum magnitude value of the target image x , $L = \max(|x|)$. We used $\beta = 0.5$ to balance the two loss functions.

For both single-coil and multi-coil MRI reconstruction tasks, we trained models with the same network architecture except the input and output dimensions and the number of feature maps of each module are different. The number of iterations for all convRNN is set to 5. All training images were center cropped to (320×320) and normalized by dividing the mean of the undersampled image. We used the lookahead version of Adam optimizer Zhang et al. [2019] with $k = 5$ and $\alpha = 0.5$. The learning rate was set to 10^{-5} for the first epoch as the training warmup and increased to 10^{-4} , which was then reduced by a factor of 2 every 10 epochs. The network was trained for 60 epochs. We simulated k-space measurements using the sampling mask function from Zbontar et al. [2018] with 4x and 8x acceleration factors.

For comparison, we also reconstructed the same data using CS and UNet as in Zbontar et al. [2018]. The code with default parameters from fastMRI github (<https://github.com/facebookresearch/fastMRI>) was adopted except that for UNet, we trained separated models for 4X and 8X acceleration in each task. PSNR and SSIM were calculated as evaluation metrics for comparison.

3 Results

We trained and evaluated our proposed model on the fastMRI dataset and compared our model with the CS based method and the deep learning based method (UNet). Table 1 shows the results evaluated on the fastMRI validation dataset. In the single-coil task, PC-CRNN outperforms CS by 3.3 and UNet by 0.9 in PSNR at 4X acceleration. At 8X acceleration, our model improves PSNR by 4.3 and 1.4 compared with CS and UNet, respectively. In the multi-coil task, the improvement is more significant. Comparing PC-RNN to the other two methods, PSNR is boosted by 8.9 and 5.3 at 4X acceleration as well as 8.3 and 2.8 at 8X acceleration. SSIM also shows consistent improvement results. Table 2 shows the PC-CRNN results on the fastMRI test dataset from the competition website. The submitted

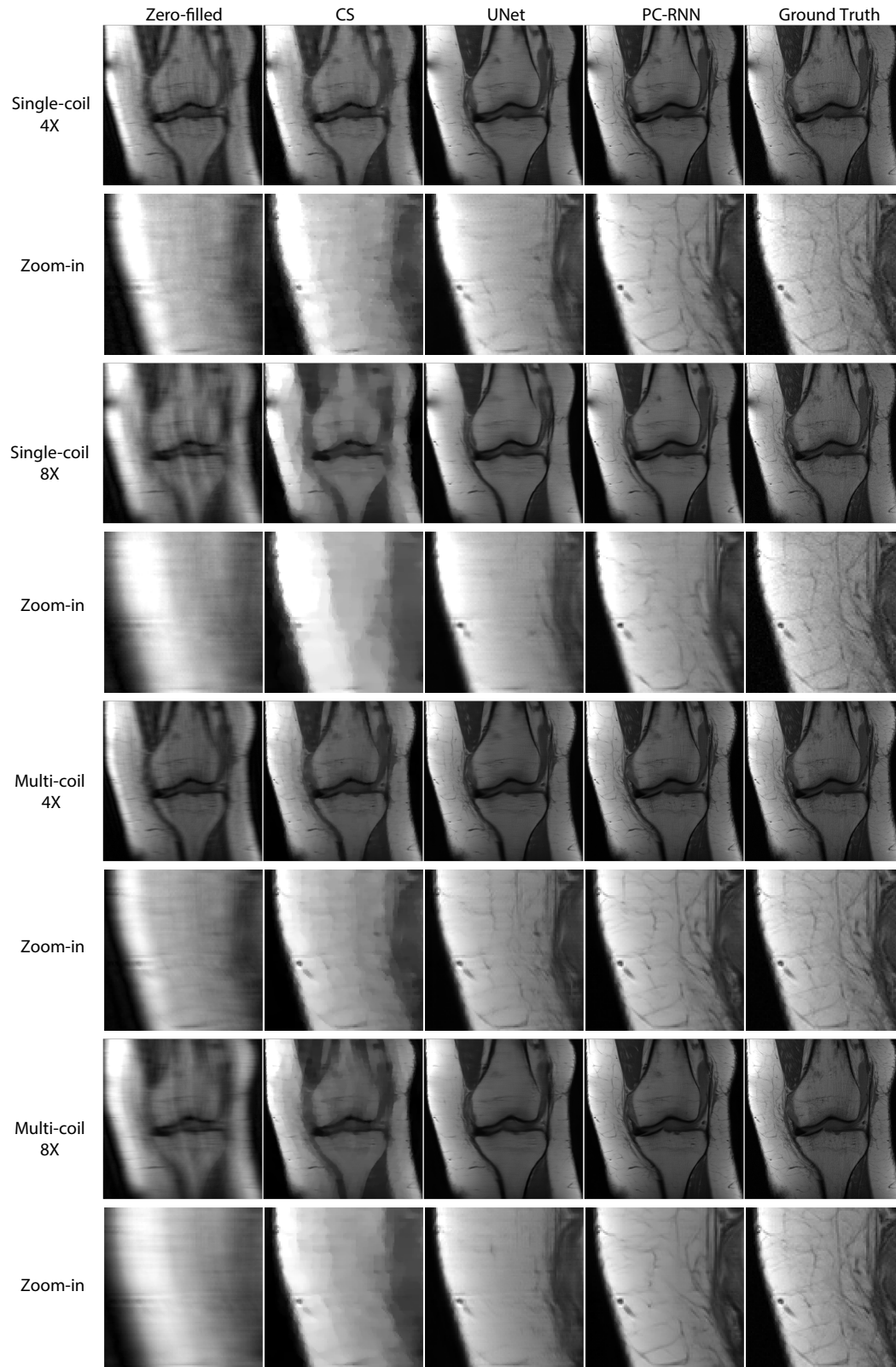


Figure 2: Examples of reconstruction results. ESC is used as the ground truth in single-coil data and RSS is used as ground truth in multi-coil data. The middle left part of each image is shown as the zoom-in image.

results were also evaluated and scored by seven radiologists. Our results rank as one of the three best submissions [Murrell et al., 2019].

Figure 2 demonstrates examples of reconstructed images by PC-RNN and other methods. Our model recovers more details, especially using multi-coil data. At 8X high acceleration, our model can reconstruct considerably more fine details than the other two methods. The reconstructed images from PC-RNN have less noise than ground truth.

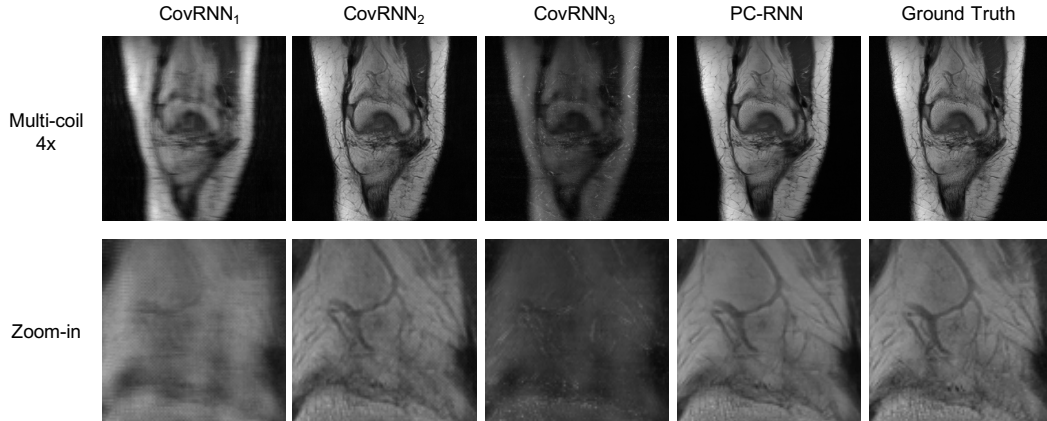


Figure 3: Intermediate and final outputs of PC-RNN and ground truth MR image. Outputs from ConvRNN_1 , ConvRNN_2 and ConvRNN_3 show that PC-RNN reconstructs images at coarse to fine scales.

To demonstrate the effectiveness of PC-RNN, we show the intermediate outputs from each ConvRNN as well as the final reconstructed image and compared them with the ground truth in Figure 3. From ConvRNN_1 to ConvRNN_3 , more and more fine structures are recovered in the reconstructed images. Furthermore, the outputs of ConvRNN_1 and ConvRNN_3 can be seen as over-smoothed and over-sharpened reconstructions. The final CNN in PC-RNN combines all three reconstructed images and outputs a balanced MR image.

4 Discussion and Conclusion

In this paper, we proposed a pyramid convolutional RNN model for MRI image reconstruction. The model reconstructs the image in various scales and then combines the coarse to fine images as the final reconstructed image. We trained and evaluated our model on the fastMRI dataset. The results show that our model can reconstruct more fine details in the image and outperforms CS and UNet in both single-coil and multi-coil tasks with 4X and 8X accelerations.

In the current model, we only implemented three different scales (1X, 2X, and 4X). The model can be extended to include more different scales in the framework of the proposed method.

References

- Jens M Edmund and Tufve Nyholm. A review of substitute ct generation for mri-only radiation therapy. *Radiation Oncology*, 12(1):28, 2017.
- Richard G. Weekes, Thomas H. Berquist, Richard A. McLeod, and William D. Zimmer. Magnetic resonance imaging of soft-tissue tumors: Comparison with computed tomography. *Magnetic Resonance Imaging*, 3(4):345–352, 1985. ISSN 0730725X. doi: 10.1016/0730-725X(85)90398-4.
- Michela Lecchi, Piero Fossati, Federica Elisei, Roberto Orecchia, and Giovanni Lucignani. Current concepts on imaging in radiotherapy. *European journal of nuclear medicine and molecular imaging*, 35(4):821–837, 2008.
- Emmanuel J Candès, Justin Romberg, and Terence Tao. Robust uncertainty principles: Exact signal reconstruction from highly incomplete frequency information. *IEEE Transactions on information theory*, 52(2):489–509, 2006.

- Shiqian Ma, Wotao Yin, Yin Zhang, and Amit Chakraborty. An efficient algorithm for compressed mr imaging using total variation and wavelets. In *2008 IEEE Conference on Computer Vision and Pattern Recognition*, pages 1–8. IEEE, 2008.
- Jong Chul Ye. Compressed sensing mri: a review from signal processing perspective. *BMC Biomedical Engineering*, 1(1):8, 2019.
- Michael Lustig, David Donoho, and John M Pauly. Sparse mri: The application of compressed sensing for rapid mr imaging. *Magnetic Resonance in Medicine: An Official Journal of the International Society for Magnetic Resonance in Medicine*, 58(6):1182–1195, 2007.
- Jeffrey A Fessler. Optimization methods for mr image reconstruction. *arXiv preprint arXiv:1903.03510*, 2019.
- Alexander Selvikvåg Lundervold and Arvid Lundervold. An overview of deep learning in medical imaging focusing on mri. *arXiv preprint arXiv:1811.10052*, 2018.
- Chen Qin, Jo Schlemper, Jose Caballero, Anthony N Price, Joseph V Hajnal, and Daniel Rueckert. Convolutional recurrent neural networks for dynamic mr image reconstruction. *IEEE transactions on medical imaging*, 38(1):280–290, 2018.
- Gil Keren and Björn Schuller. Convolutional rnn: an enhanced model for extracting features from sequential data. In *2016 International Joint Conference on Neural Networks (IJCNN)*, pages 3412–3419. IEEE, 2016.
- Xingjian Shi, Zhouong Chen, Hao Wang, Dit-Yan Yeung, Wai-Kin Wong, and Wang-chun Woo. Convolutional lstm network: A machine learning approach for precipitation nowcasting. In *Advances in neural information processing systems*, pages 802–810, 2015.
- Jure Zbontar, Florian Knoll, Anuroop Sriram, Matthew J Muckley, Mary Bruno, Aaron Defazio, Marc Parente, Krzysztof J Geras, Joe Katsnelson, Hersh Chandarana, et al. fastmri: An open dataset and benchmarks for accelerated mri. *arXiv preprint arXiv:1811.08839*, 2018.
- Michael R Zhang, James Lucas, Geoffrey Hinton, and Jimmy Ba. Lookahead optimizer: k steps forward, 1 step back. *arXiv preprint arXiv:1907.08610*, 2019.
- Tullie Murrell, Nafissa Yakubova, Anuroop Sriram, Mike Rabbat, and Larry Zitnick. Results of the first fastmri image reconstruction challenge. <https://ai.facebook.com/blog/results-of-the-first-fastmri-image-reconstruction-challenge/>, 2019.

Table S1: Details of proposed network architecture for single-coil MRI reconstruction. For multi-coil task, the number of feature maps of 4 modules are increased to 512, 256, 128 and 128 accordingly.

Module	Block	Type	Output size
Input image	–	–	$2 \times 320 \times 320$
ConvRNN ₁ -4x	Encoder	Conv(2,4,1)	$384 \times 160 \times 160$
		Conv(2,4,1)	$384 \times 80 \times 80$
	ResBlock	ResConv	$384 \times 80 \times 80$
		ResConv	$384 \times 80 \times 80$
Decoder	DeConv(2,4,1)	$384 \times 160 \times 160$	
		DeConv(2,4,1)	$2 \times 320 \times 320$
ConvRNN ₂ -2x	Encoder	Conv(1,3,1)	$192 \times 320 \times 320$
		Conv(2,4,1)	$192 \times 160 \times 160$
	ResBlock	ResConv	$192 \times 160 \times 160$
		ResConv	$192 \times 160 \times 160$
Decoder	DeConv(2,4,1)	$192 \times 320 \times 320$	
		DeConv(1,3,1)	$2 \times 320 \times 320$
ConvRNN ₃ -1x	Encoder	Conv(1,3,1)	$96 \times 320 \times 320$
		Conv(1,3,1)	$96 \times 320 \times 320$
	ResBlock	ResConv	$96 \times 320 \times 320$
		ResConv	$96 \times 320 \times 320$
Decoder	DeConv(1,3,1)	$96 \times 320 \times 320$	
		DeConv(1,3,1)	$2 \times 320 \times 320$
CNN	–	Conv(1,3,1)	$6 \times 320 \times 320$
		Conv(1,3,1)	$96 \times 320 \times 320$
		Conv(1,3,1)	$96 \times 320 \times 320$
		Conv(1,3,1)	$2 \times 320 \times 320$
Output image	–	–	$2 \times 320 \times 320$
	ResConv	Input	$C \times M \times N$
		Conv(1,3,1)	$C \times M \times N$
		Conv(1,3,1)	$C \times M \times N$